Two-Sites Are Better Than One: Revisiting the OER Mechanism on CoOOH by DFT with Electrode Polarization.

Antton Curutchet[1], Pauline Colinet[1], Carine Michel[1], Stephan N. Steinmann[1], Tangui Le Bahers[1]**

[1]Univ Lyon, ENS de Lyon, CNRS, Université Lyon 1, Laboratoire de Chimie UMR 5182, Lyon, France

Corresponding Author

* authors for correspondence: stephan.steinmann@ens-lyon.fr, tangui.le_bahers@ens-lyon.fr

ABSTRACT

In this work, we uncover the existence of several competitive mechanisms of water oxidation on the β-CoOOH (10-14) surface by going beyond the classical 4-step mechanism frequently used to study this reaction at the DFT level. Our results demonstrate the importance of two-site reactivity and of purely chemical steps with the associated activation energies. Taking the electrochemical potential explicitly into account leads to modifications of the reaction energy profile finally leading to the proposition of a new family of mechanisms involving tetraoxidane intermediates. The two-site mechanisms revealed in this work are of key importance to rationalize and predict the impact of dopants in the design of future catalysts.

TOC Graphic

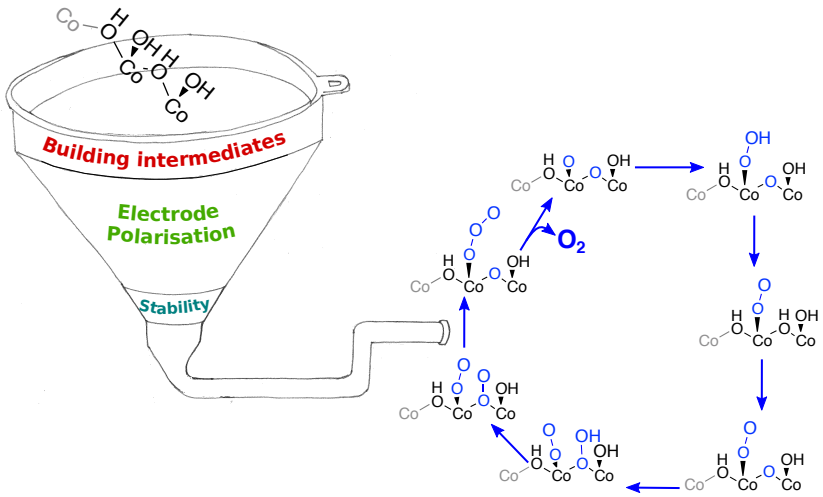

Key word list:

CoOOH, water oxidation, DFT, electrode polarization, mechanism, Poisson-Boltzmann, CHE

1. Introduction

The replacement of fossil energy production by renewable energies is a pressing topic. Besides the massive cost for a change in infrastructure, the storage of electrical energy is the missing link for intermittent wind and solar energies to take over the lead of global energy production. In this field, the most trending solution is chemical energy storage, among which water-splitting to produce hydrogen is the most viable option.[1] The development of hydrogen production from electrochemical water splitting is mainly limited by the activity of the catalyst used to perform water oxidation, also called Oxygen Evolution Reaction (OER).[2]

For years noble metal-based catalyst such as IrO_2 or RuO_2 were reported as the most efficient OER catalysts[3–5] but in the last decade, some earth-abundant first row transition metal catalysts have become competitive[6–10]. CoOOH and NiOOH-based catalysts are the most promising ones, with overpotentials as low as 0.19 V.[11–13] Unlike iridium and ruthenium-based catalysts, these oxyhydroxides work at alkaline pH. Despite the efficiency of these recent catalysts, the OER mechanism is unclear, and still an important topic of investigation, even for pristine oxyhydroxides, which hampers the development of new OER catalysts within this family.[10,14–17]

Computational protocols, mainly based on Density Functional Theory (DFT), have shown their usefulness to bring an atomistic point of view on these mechanisms to support and guide the development of new catalysts. Frequently, the DFT based works focus on a single site 4-step mechanism to determine the overpotential of the OER reaction on a given catalyst surface. Starting from a hydroxylated surface, the 4-step mechanism in basic conditions reads:

$$^{*}\mathbf{OH} + \mathbf{OH^-} \rightarrow {}^{*}\mathbf{O} + \mathbf{H_2O} + \mathbf{e^-} \qquad \text{(step 1)}$$

$$^{*}\mathbf{O} + \mathbf{OH^-} \rightarrow {}^{*}\mathbf{OOH} + \mathbf{e^-} \qquad \text{(step 2)}$$

$$^{*}\mathbf{OOH} + \mathbf{OH^-} \rightarrow * + \mathbf{O_2} + \mathbf{H_2O} + \mathbf{e^-} \qquad \text{(step 3)}$$

$$\mathbf{OH^-} + * \rightarrow {}^{*}\mathbf{OH} + \mathbf{e^-} \qquad \text{(step 4)}$$

As we demonstrate herein, this 4-step mechanism hides the complexity of the real mechanism that, in general, contains formally chemical steps and can involve several sites.[18] Such a multi-site

reactivity has previously been reported for other oxides[4,19–23] and a first computational investigation has been performed on CoOOH to determine the influence of an oxygen vacancy[20], highlighting the necessity to consider more complex reaction paths than the typical one-site 4-step mechanism.

In this work, we investigate the water oxidation over β-CoOOH. This model catalyst is representative of the promising oxyhydroxy catalyst family for water oxidation.[11,24] Furthermore, to be consistent with experimental conditions, the global reaction used in this work correspond to alkaline pH: $4OH^- \rightleftharpoons 2H_2O + O_2 + 4e^-$. The objective is to complete the energy landscape of the OER on this material, going beyond the single-site, 4-step mechanism. Such a comprehensive mechanism allows to direct future screening studies for doped materials and identifies key intermediates which could be experimentally observed. Inspired by the work of Ping *et al.*,[4] we herein extend the use of electrode polarization in the DFT modelling of electrochemical reactions to semiconducting, spin-polarized materials (compared to metallic, diamagnetic systems in previous works). Our work thus offers an understanding of the effect of the electrochemical potential on the reaction mechanism even on surfaces with complex electronic structures.

2. Methodology

Our study is based on a systematic selection of intermediates and simulates the impact of the electrochemical potential explicitly in conjunction with a continuum model for the water solvent and electrolyte.

2.1 Computational details.

All calculations were carried out within the context of periodic density functional theory (DFT), as implemented in the Vienna Ab-initio Simulation Package (VASP), version 5.3.5.[25–28], with the PBE GGA functional.[29] The core electrons were described by using the projected-augmented plane-wave (PAW) pseudopotential. The k-point sampling of the first Brillouin zone was done with a 3x2x1 Monkhorst-Pack grid for slab calculations and 12x12x12 grid for bulk calculations. The cut-off energy of the plane wave was set to 600 eV and the energy convergence criterion for the self-consistent-field (SCF) cycles was set to 10^{-6} eV per cell. To validate the convergence of the basis set size, the

mechanism **I** (presented after in the text) was computed in the CHE model with a 700 eV cutoff. Reaction energies varied by less than 10 meV supporting the choice of 600 eV cutoff of this study. Hubbard Hamiltonian (denoted +U) was added in the calculations to improve the description of the electronic structure of this strongly correlated material. On the basis of previous works, the formalism proposed by Dudarev et al.[30] was used, along with the U-J value of 3.52 eV for the cobalt 3*d* electrons.[31–33] Dispersion interactions were included along with the dDsC model.[34,35]

Preliminary bulk full relaxation was operated on β-CoOOH (R-*3m* space group), as it was proved to be the most active phase of cobalt oxide at alkaline pH and oxidative conditions.[32,36] The reference slab was a 3x2 supercell of the primitive surface cell obtained by cutting bulk β-CoOOH in the most active (10-14) direction as reported by Bajdich et al.[8] A thickness of four layers (i.e. containing four Co planes) was kept as it showed a converged value of surface energy, and all surface Co atoms were linked to hydroxyl groups to complete their octahedral surrounding shell. Inversion symmetry was kept in all calculations in order to have no dipole momentum. To validate the choice of the slab thickness, the reaction energies of the mechanism **I** were computed in the CHE model on slab containing 6 layers of Co atoms. The largest change in reaction energies was 24 meV compared to the 4 layers slab used for this work, supporting the reliability of the results obtained with a 4 layers model of the β-CoOOH surface.

During the geometry relaxations of the surface, only the outer atoms were allowed to relax, while the cell parameters and inner atoms (in a 2 Å-large middle layer) were fixed to those determined on the bulk β-CoOOH. These relaxations were operated until the residual forces were below 0.02 eV.$Å^{-1}$. Electronic occupancies were determined by a Fermi smearing of 0.026 eV, corresponding to a temperature of 298 K (which is the expected working temperature.)

All systems were obtained by modifying the termination of surface Co atoms from the reference slab. For each system, several possible geometry configurations and several spin states were investigated to find the most stable ones.

The energies of H_2 and H_2O were computed in a cell of same 3x2 dimensions without the surface, and same other computational parameters. To avoid the calculation of the O-O bond energy, which is

poorly estimated at the DFT-GGA level, the Gibbs energy for the formation of a water molecule has been set to 1.23 eV.

Accounting for solvation effects is achieved by exploiting the implicit solvation mode as implemented by Hennig and co-workers under the name VASPsol.[37–39]

Electrochemical potential was modified by a surface-charging method based on the linearized Poisson-Boltzmann (PB) equation implemented in VASPsol by the Hennig group.[38,39] This equation allows us to include an idealized electrolyte distribution in the electronic structure computations. This electrolyte distribution also serves to balance the surface charge without the need for any correction terms, in contrast to the surface-charging model assuming a homogeneous background charge.[40] A more detail description of the corresponding methodology can be found here.[41]

The transition states (TS) have been located as follows: the initial and final states were built by physisorption of molecules when necessary. Then, a rough nudged-elastic band (NEB)[42] computation with 8 images between the initial and final state was performed, seeded by linear interpolations between the two states. After 30 cycles of NEB, an improved guess for the transition state was obtained, which was refined by the quasi-Newton or dimer method[43–45] and verified to be a first-order saddle point by a frequency analysis.

While the zero-point energy were not included (given the number of intermediates and to the fact that the variation in ZPE was found small in our previous work on this system[33]), the energies reported in this work obtained from the electrode polarization analysis can be considered as free energies because we are dealing here with a grand canonical description of the electrons. But to avoid confusions with free energies that include thermal (entropy) corrections, which are more common in computational chemistry, we will refer to "energy" and not free energy in the text.

2.2 A systematic approach to build the reaction path.

Figure 1 presents the structure of the β-CoOOH (10-14) hydrated surface, where all Co atoms are equivalent and each one linked to three OH groups. Two of these OH groups are bridging with another Co atom (μ_2 coordination), while the third one is bound to only one Co (terminal μ_1

coordination). The most frequently used reaction path in the literature for water oxidation involves the use of only one terminal OH group.[10,46,47] In this work, we systematically investigate the possibility to use 2 different OH groups. Considering the very large number of intermediates that would derive from 3 OH groups, the impact of a third site is only considered for some selected intermediates.

Generally, a 4-step OER mechanism is reported for this material.[32,33] Wang *et al.* were among the firsts to propose the idea that multi-site reactivity should be considered for CoOOH involving an oxygen vacancy.[20] To go beyond the mechanism proposed by Wang *et al*. and reach a more realistic description of the OER mechanism, we applied a systematic approach probing a larger number of intermediates without any initial assumption on their stability. This approach is detailed in the following.

Starting from the reference structure (i.e. the fully hydroxylated, β-CoOOH (10-14) surface) denoted **A**, all possible intermediates involving one of the four OH groups mentioned previously (See Figure 1) were built. The allowed chemical reactions are: addition of H_2O or HO^-, and removal of H^+ or O_2. This leads to 75 possible intermediates (see Table S1). The geometry optimization converged to the expected intermediate for 56 of them. To focus on the most relevant reaction intermediates, all isomers with a relative energy above 0.5 eV compared to the most stable ones are discarded (see Figure S1), since at room temperature, the likeliness of reaching those isomers is already very limited. Transitions states were considered only for water dissociation and O_2 formation and not for electrochemical steps. The characteristic of electrochemical steps lies in the change of total number of electroactive species during the step (change in proton number in our case) making the definition of a transition state ambiguous. Some attempts have been proposed in the literature[48–50] to compute transitions states of electrochemical steps but these approaches are up to now more a proposition of methodology than a well-accepted scheme, justifying our choice not to model the activation energies of these specific steps. Similarly, to intermediates, transition states for water dissociation and O_2 desorption are discarded if they are higher than 0.5 eV compared to the lowest one for a given reaction, a threshold that limits the number of investigated routes and allowed us to identify several accessible pathways. For more details on transition states see Supporting Information. The explicit impact of the electrochemical potential was assessed only for this selection of 44 intermediates and

transition states. This impact is simulated by computing the energy as a function of the chemical potential. The chemical potential of the system is tuned by charging the slab using an approach called "surface charging" or "grand canonical DFT" and is associated with a Poisson-Boltzmann electrolyte for the charge compensation. This scheme has been previously used by the authors for metallic surfaces and is well documented in the following references.[51–53] As discussed in the following paragraphs, this systematic selection results in several OER mechanisms, with overpotentials (η) that depend on whether the electrochemical potential is included at the CHE level (η_{CHE}) or through surface charging and a Poisson-Boltzmann electrolyte (η_{PB}).

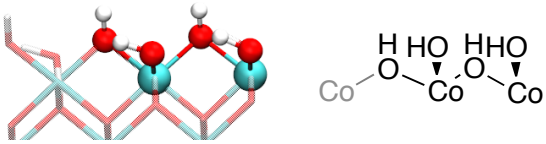

Figure 1: Two representations of the CoOOH reference (10-14) surface (**A** structure), showing μ_2 and terminal OH groups. Atoms in cyan, red and white correspond to cobalt, oxygen and hydrogen respectively.

3. Results and Discussion

3.1 CHE results

At the CHE level, the selection of intermediates with the 0.5 eV cutoff explained previously lead to 33 intermediates distributed in three mechanisms. Figure 2 shows the best reaction path for each mechanism. Only 15 of the 33 intermediates are displayed for simplicity, as the 18 remaining ones are configuration isomers (all intermediates and corresponding mechanisms are shown in the SI). Mechanism **I** occurs on only one OH-site (intermediates **A**, **B**, **C**, **D**, **E**), while mechanisms **II** and **III** (intermediates **1**, **1'**, **2**, **2'**, **3**, **3'**, **4**, **5'**, **6'**) involve 2 OH-sites. In term of notation, the relation between a number and a number with a prime is just an isomerization. The considered 3-OH based intermediates are all discarded by the 0.5 eV criterion.

The only possible reaction of the hydroxylated reference surface state **A** is an oxidation according to step 1 of the 4-step mechanism shown above. This oxidation (**A→B**) creates a Co=O

termination, liberating the first electron and proton pair and is formally equivalent to a dehydrogenation. Intermediate **B** can be further oxidized by a hydroxide ion (step 2, i.e., **B→C**), which liberates the second electron. After a second coupled proton-electron transfer (step 3, **C→D**), generating the third electron, oxygen is desorbed (**D→E**) in a chemical step. Finally, a second hydroxide ion regenerates the reference structure **A** and liberates the fourth electron (step 4, **E→A**). This first path, called mechanism **I** and shown in green in Figure 2, is very similar to the common 4-step mechanism (**A→B→C→E**, shown by green squares), except that the last step (**C→E**) actually consists of a proton/electron exchange step (**C→D**) and a non-electrochemical O_2-dissociation step (**D→E**).

A first alternative to this mechanism appears when a second site is involved: From intermediate **B** the dehydrogenation of a neighboring μ_2 OH site can lead to intermediate **1**, which can react in a similar way as **B** leading to mechanism **II** shown in red in Figure 2: OH^- uptake by the terminal oxygen of **1** gives intermediate **2**, which isomerizes to **D**. Then another dehydrogenation leads to **3** from which oxygen is able to desorb (**3→4**). Eventually, addition of hydroxide (**4→B'**) regenerates intermediate **B** after a last isomerization (**B'→B**). It is worth noting that intermediate **A** is not in this catalytic cycle, thus **A→B** is an initiation process for this mechanism.

Another pathway branches from intermediate **D** to form **3'** (**D→3'**), where a second O-O bond can be created by OH^- addition (**3'→5'**). This leads to mechanism **III** (in blue in Figure 2) involving a tetraoxidane ring intermediate **6'**. This tetraoxidane structure has never been described in literature for this catalysts to the authors' knowledge but similar peroxo species has been reported both theoretically[19,54] and experimentally.[23,54,55] Mechanism **III** cycles over intermediate **D**, invoking **A→D** only as an initiation process. Interestingly, this cycle has only one intermediate in common with the first mechanism, and involves none of the common intermediates of the 4-step mechanism **A**, **B**, **C**, **E** (except in initiation phase).

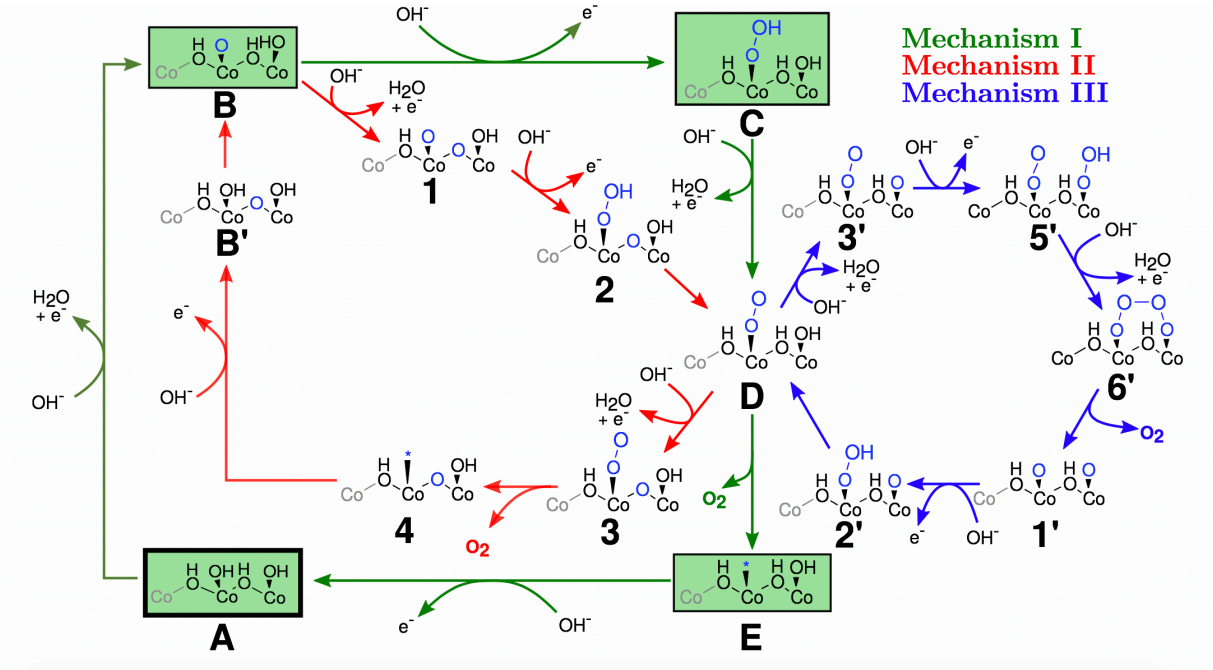

Figure 2: three mechanisms in competition for water oxidation. The 4 intermediates frequently reported in literature are highlighted in green. A comprehensive mechanism involving configuration isomers of the intermediates displayed here is shown in the SI.

Figure 3 shows the energies of the reaction intermediates shown in Figure 2, computed in the CHE approach, at η=0.57 V. The electrochemically-limiting steps of mechanisms **I**, **II** and **III** are **B→C**, **1→2**, and **D→3'** respectively, and set the CHE overpotential value to 0.57 V, 0.57 V and 0.59 V respectively. Mechanism **I** and **II** seem very similar as they have the same overpotential value given by a chemically similar step (first creation of O-O bond). But an important difference is noted when comparing the non-electrochemical O_2-dissociation steps. **D→E**, is endothermic, which means that no matter the applied overpotential, mechanism **I** keeps an activation barrier of 0.3 eV. This was not observed in the study by Bajdich *et. al.*[54] as intermediate **D** was not considered. Instead, O_2-dissociation step of mechanism **II**, **3→4**, is fully exothermic except the 0.03 eV isomerization barrier **B'→B**. This difference is due to the stabilisation of the pentacoordinated cobalt in **4** by the stronger bonding with the dehydrogenated neighbouring oxygen (Co-O distance 1.74 Å), compared to the hydroxyle in same position in **E** (Co-O distance 1.98 Å). Last, in mechanism **III**, the electrochemical step **D→3'** features a 0.02 eV barrier at 0.57 V, which is compensated by increasing the overpotential

to 0.59 V, and no other step is endothermic, including O_2 dissociation. Mechanism **III** is, therefore, more efficient than mechanism **I**, and more efficient than mechanism **II** at slightly higher potentials. These competing pathways illustrate that considering CHE overpotential is not sufficient to determine the best mechanism when non-electrochemical steps come into play. Furthermore, the single-site 4-step mechanism frequently used in the literature to understand the water oxidation on several oxides, including CoOOH, is not the most adapted one. Multi-site mechanisms (here **II** and **III**) appear to be more competitive. According to experiments, doped CoOOH and bimetallic oxyhydroxides (such as (Fe,Co)OOH) lead to lower overpotentials for OER compared to pure CoOOH.[33,54] However, the one site mechanism can fail to reproduce the ordering of overpotential for (M,Co)OOH. [24,54] A complete multi-site investigation might recover the experimental trends regarding the overpotentials and thus offer a way to a rational design of improved catalysts. It is interesting to note that, all three mechanisms obtained in this work present peroxo intermediates, experimentally characterized during OER.[15]

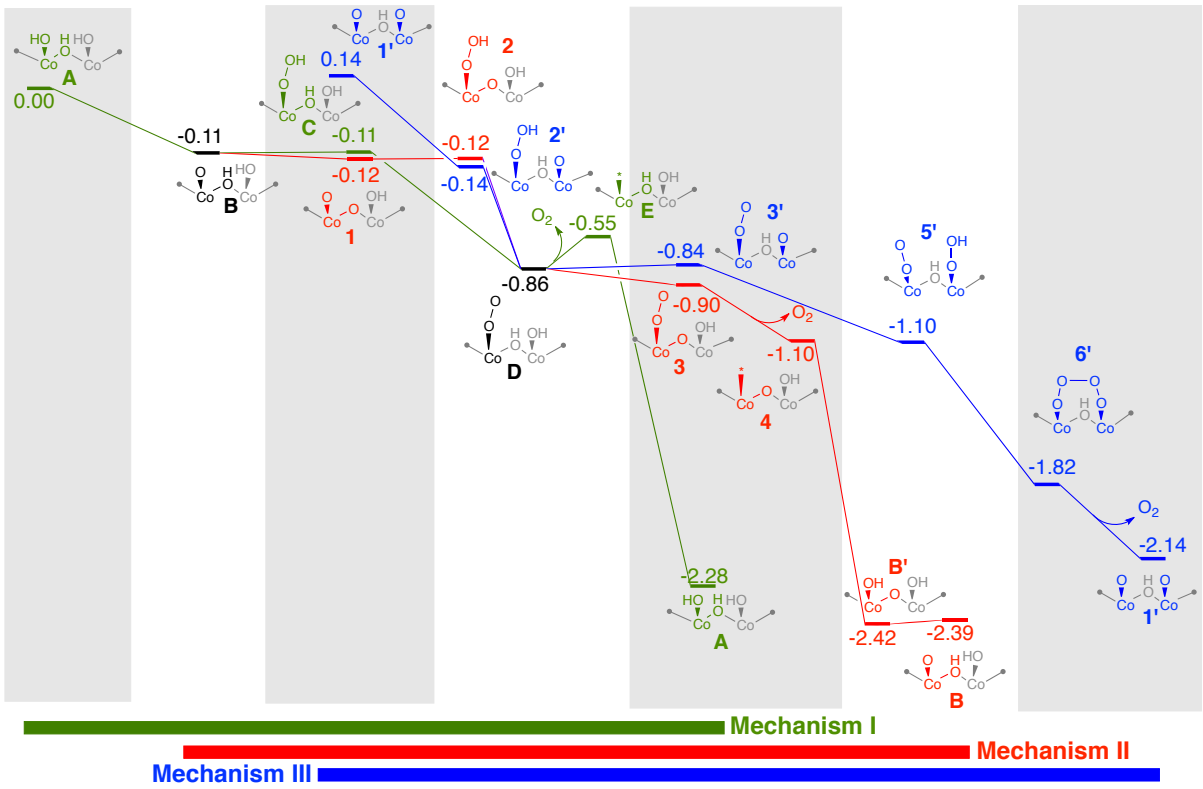

Figure 3: CHE energies of intermediates of the three mechanisms shown in Figure 2 at 0.57 V overpotential. Grey and white vertical stripes refer to different oxidation states.

3.2 Inclusion of electrochemical potential and transition states.

These results at the CHE-level are compared to results with explicit inclusion of the electrochemical potential (PB-level) along with inclusion of transition state (TS) computation for some selected chemical steps. The potential area of interest is 1.80 V/RHE (0.57 V overpotential). As a first result, the consideration of TS changes slightly the conclusion. Mechanism **III** experiences a large activation barrier for opening of the tetraxoxidane ring (Figure 4(a)). However, an analogue to mechanism **III** that passes through different isomers, does not have such high activation energy. The most important feature of this mechanism **IV** is presented in Figure 4(a) and is fully depicted in Figure S2. Since mechanism **IV** is also characterized by the presence of tetraoxidane ring, mechanism **III** is replaced by mechanism **IV** in the discussion from now on.

As summarized in Figure 4, the energy correction due to the explicit inclusion of the electrochemical potential (PB) is negligible (<0.1 eV) for most limiting steps. Just like in one of our previous study[56], the chemical steps (Figure 4(b)) are more sensitive to the explicit inclusion of the electrochemical potential than the electrochemical steps. The largest change in the reaction energy is observed for the **D→E** reaction, which corresponds to the O_2 desorption, which shifts from endo to exothermic upon the explicit inclusion of the potential, removing the thermodynamic barrier computed in CHE. The reason of this large change can be understood from the energy of each of these two intermediates as a function of the overpotential, drawn in Figure 5. When working at neutral charge in the CHE model, the **E** intermediate is found higher in energy than the **D** one. To reach the overpotential of the OER reaction, it is necessary to apply a much larger charge to the **E** intermediate, lowering the energy of this intermediate significantly and leading to a **D→E** reaction energy of opposite sign. The difference in the charge that must be applied to **D** and **E** to reach the OER overpotential can be traced back to the difference in the Fermi level, which is notably higher in the **E** intermediate (~ -4.3 V vs vac) compared to the **D** intermediate (~ -5.0 V vs vac). Consequently, the **E** intermediate must be strongly oxidized to reach the same Fermi level of the **D** intermediate to obtain the overpotential at constant potential condition (PB model). Chemically, a higher Fermi level of the **E** intermediate is due to the shift from a low spin state for the surface Co in **D** (no spins computed on the Co atoms) to a high spin

state of the pentacoordinated Co atom in **E** (computed to be 2.7 μ_B). This conclusion can be extended to all intermediates containing pentacoordinated Co atoms, all being in a high spin state, such as intermediates **4** and **E** and also for **4'**, **4''**, **4'''** presented in SI. All of them are characterized by a pentacoordinated cobalt atom and they are stabilized by up to 0.6 eV compared to the CHE result. Hence, the elementary steps involving these intermediates are significantly altered by the inclusion of the electrochemcial potential. A more realistic solvent description could eventually affect this energy stabilization. However, explicit solvent and micro-solvation are extremely difficult to manage when building reaction networks and can lead also to artefacts.[57,58] While not perfect, the implicit solvent approach is already assumed to be a good starting point to investigate solvent influence, as concluded by Van den Bossche *et al.* in their study of H_2 evolution reaction of Pt surfaces.[48]

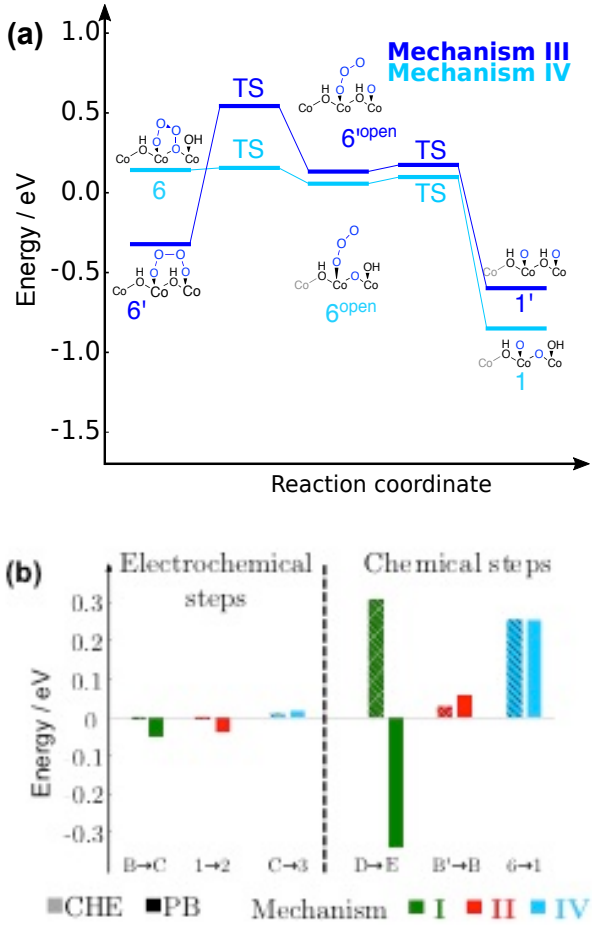

Figure 4: (a) Detailed reaction profiles of O_2 desorption step for two different configurations involved in mechanisms **III** and **IV**. (b) Comparison between CHE and PB approaches on the energy of kinetically determining steps at 0.57 V overpotential.

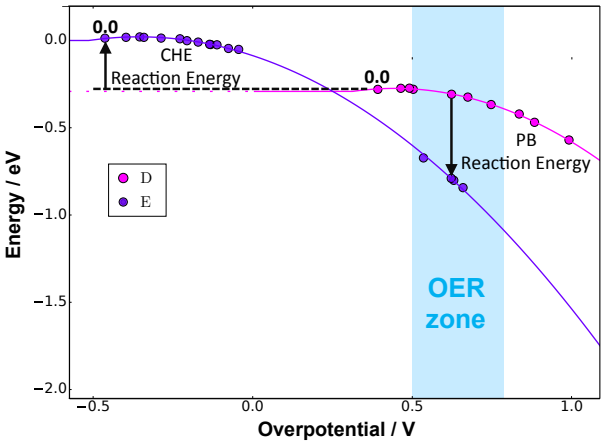

Figure 5: Energy of the **D** and **E** intermediates (points are computed energies at different charge, lines are fitted curves) as a function of the OER overpotential. The "0.0" notation indicate the points of neutral charge used in the CHE methodology.

Mechanism	Overpotential (V)	Associated Step	Chemical Barrier (eV)	Associated Step
I	0.68	**A→B**	n.a.	n.a.
II	0.55	**B→1**	0.06	**B'→B**
IV	0.55	**1→2**	0.26	**6→6°**

Table 1: Final comparison of different mechanisms, with inclusion of transition states and polarization.

It is interesting now to compare the results from the CHE and the PB models. From a global point of view, the overpotentials of 0.57 V, 0.57 V, 0.59 V in and CHE becoming 0.68 V, 0.55 V, 0.55 V in PB for mechanisms **I**, **II** and **III** (or **IV**) respectively seem to be not dramatically affected by the inclusion of the potential. But qualitatively, the inclusion of the potential (i.e. the PB model) changed mainly the idea we can have about the reaction. First the mechanism **I** is no longer the most favorable one, overpassed by mechanism **II** and **IV** indicating that a multi-site reactivity is favorized. But also, the nature of rate determining steps has changed. Thus, attempts of improvement of OER catalysts based on the rate determining steps found by the CHE model will not necessarily succeed.

Experimentally, the overpotential measured for the CoO_x system (assumed to be CoOOH) is generally reported to be around 0.30-0.40 V.[11,20,24,33,59] The comparison to experiment is more difficult because the overpotential extracted from electrocatalysis is generally defined as the extra potential applied to obtain a certain current density (usually 10 $mA.cm^{-2}$). Thus, the experimental definition of the overpotential is not the same as the computational one. Even if these two overpotentials are related and probably correlated, there is no reason to think they will be equal. We can just note that the overpotential computed by the CHE approach or by the PB approach are numerically relatively close to the experiment. The validation of the mechanisms found by calculation on the basis of the agreement between calculated and measured overpotentials is thus impossible. Two other ways could be considered to validate the theory. First, a multiscale modelling using the mechanisms found at the DFT level in a micro-kinetic model cold be used to simulate a J-V curve leading to an estimation of the overpotential on the basis of current threshold as it is done experimentally. Another way could be to characterize experimentally some of the intermediates proposed in the mechanisms such as the tetraoxidane.

4. Conclusion

By using a systematic approach to build the intermediates and by improving the description of the energy profile of several mechanisms by including transition states and polarization induced by the electrochemical potential, three mechanisms of water oxidation on the β-CoOOH (10-14) hydrated surface have been identified. Mechanism **I** is similar to the standard 4-step mechanism frequently used in the literature but with an additional purely chemical step. Mechanism **II** changes from the mechanism **I** by the involvement of two sites for water oxidation. Mechanism **IV** is also a two sites mechanism but involving tetraoxidane intermediates. The overpotential and activation energies (for the chemical steps) of the three mechanisms are gathered in the Table 1. Coincidentally, mechanism **I**, which is based on the popular 4-step mechanism, is not the most favorable one. This mechanism is overpassed by the mechanism **II** having the lowest overpotential and almost no activation energy for chemical steps. While the activation energy of mechanism **IV** is the largest of the three, its relatively weak value allows us to consider this reaction path, and the tetraoxidane associated, as a reasonable

one. Experimental effort could be devoted to characterize the existence of such tetraoxidane species to support the existence of mechanism **IV**.

Among all the improvements done in the work compared to the 4-step CHE approach, the most important one turned out to be the inclusion of multi-site mechanism shining light on the necessity to improve our chemical understanding of the reactivity of oxyhydroxide electrocatalyst. The computationally demanding PB-model appears to be an improvement compared to CHE only for the steps involving the undercoordinated cobalt. This opens the eyes on the possibility to develop an improved procedure compared to the 4-step CHE mechanism involving multi-site mechanisms and using the PB-model only to refine the energy of some selected steps to go beyond the *ab initio* based approaches proposed up to now. Such a refined computational protocol will be crucial to rationalize and predict the impact of metal doping in this class of materials.

ACKNOWLEDGEMENT

The authors thank the SYSPROD project and AXELERA Pôle de Compétitivité for financial support (PSMN Data Center). This work was granted access to the HPC resources of CINES, IDRIS and TGCC under the allocation 2018-080609 made by GENCI.

SUPPORTING INFORMATION

The Supporting Information contains: the Figure S1 illustrating the principle of 0.5 eV criterion for reaction steps; the list of all intermediates (Table S1) and all the reaction paths found (Figure S3 and Figure S4); the Figure S2 summarizing the reaction mechanisms **I**, **II** and **IV**; Information about transition state calculations and some remarks about the free energy variation as a function of electrochemical potential. The Supporting Information file ends with the full list of intermediates' structures at 0 charge given in a POSCAR format.

CONFLICT OF INTEREST

There is no conflict of interest to declare.

REFERENCES

1 M. Aneke and M. Wang, *Appl. Energy*, 2016, **179**, 350–377.

2 T. Shinagawa and K. Takanabe, *ChemSusChem*, 2017, **10**, 1318–1336.

3 L. C. Seitz, C. F. Dickens, K. Nishio, Y. Hikita, J. Montoya, A. Doyle, C. Kirk, A. Vojvodic, H. Y. Hwang, J. K. Norskov and T. F. Jaramillo, *Science (80-.).*, 2016, **353**, 1011–1014.

4 Y. Ping, R. J. Nielsen and W. A. Goddard III, *J. Am. Chem. Soc.*, 2016, **139**, 149–155.

5 A. Harriman, I. J. Pickering, J. M. Thomas and P. A. Christensen, *J. Chem. Soc., Faraday Trans.*, 1988, **84**, 2795–2806.

6 X. Yu, M. Zhang, W. Yuan and G. Shi, *J. Mater. Chem. A*, 2015, **3**, 6921–6928.

7 M. Gong and H. Dai, *Nano Res.*, 2015, **8**, 23–39.

8 J. Wang, W. Cui, Q. Liu, Z. Xing, A. M. Asiri and X. Sun, *Adv. Mater*, 2016, **28**, 215–230.

9 Y. Wang, D. Yan, S. El Hankari, Y. Zou and S. Wang, *Adv. Sci.*, 2018, **5**, 1800064.

10 F. Song, L. Bai, A. Moysiadou, S. Lee, C. Hu, L. Liardet and X. Hu, *J. Am. Chem. Soc.*, 2018, **140**, 7748–7759.

11 B. Zhang, X. Zheng, O. Voznyy, R. Comin, M. Bajdich, M. García-Melchor, L. Han, J. Xu, M. Liu, L. Zheng, F. P. G. De Arquer, C. T. Dinh, F. Fan, M. Yuan, E. Yassitepe, N. Chen, T. Regier, P. Liu, Y. Li, P. De Luna, A. Janmohamed, H. L. Xin, H. Yang, A. Vojvodic and E. H. Sargent, *Science (80-.).*, 2016, **352**, 333–337.

12 S. Zhao, Y. Wang, J. Dong, C. T. He, H. Yin, P. An, K. Zhao, X. Zhang, C. Gao, L. Zhang, J. Lv, J. Wang, J. Zhang, A. M. Khattak, N. A. Khan, Z. Wei, J. Zhang, S. Liu, H. Zhao and Z. Tang, *Nat. Energy*, 2016, **1**, 16184.

13 X. Xu, F. Song and X. Hu, *Nat. Com.*, 2016, **7**, 1–7.

14 V. Fidelsky, V. Butera, J. Zaffran and M. C. Toroker, *Theor. Chem. Acc.*, 2016, **135**, 1–5.

15 A. C. Garcia, T. Touzalin, C. Nieuwland, N. Perini and M. T. M. Koper, *Angew. Chem. Int. Ed.*, 2019, 1–6.

16 L. Trotochaud, S. L. Young, J. K. Ranney and S. W. Boettcher, *J. Am. Chem. Soc.*, 2014, **136**,

6744–6753.

17 M. W. Louie and A. T. Bell, *J. Am. Chem. Soc.*, 2013, **135**, 12329–12337.

18 N. T. Suen, S. F. Hung, Q. Quan, N. Zhang, Y. J. Xu and H. M. Chen, *Chem. Soc. Rev.*, 2017, **46**, 337–365.

19 A. J. Tkalych, H. L. Zhuang and E. A. Carter, *ACS Catal.*, 2017, **7**, 5329–5339.

20 J. Wang, J. Liu, B. Zhang, H. Wan, Z. Li, X. Ji, K. Xu, C. Chen, D. Zha, L. Miao and J. Jiang, *Nano Energy*, 2017, **42**, 98–105.

21 A. Kay, I. Cesar and M. Grätzel, *J. Am. Chem. Soc.*, 2006, **128**, 15714–15721.

22 Y. F. Li and A. Selloni, *ACS Catal.*, 2014, **4**, 1148–1153.

23 A. M. Ullman, C. N. Brodsky, N. Li, S. L. Zheng and D. G. Nocera, *J. Am. Chem. Soc.*, 2016, **138**, 4229–4236.

24 C. C. L. McCrory, S. Jung, J. C. Peters and T. F. Jaramillo, *J. Am. Chem. Soc.*, 2013, **135**, 16977–16987.

25 G. Kresse and J. Furthmüller, *Comput. Mat. Sci.*, 1996, **6**, 15–50.

26 G. Kresse and D. Joubert, *Phys. Rev. B*, 1999, **59**, 1758–1775.

27 G. Kresse and J. Hafner, *Phys. Rev. B*, 1994, **49**, 14251–14269.

28 G. Kresse and J. Furthmüller, *Phys. Rev. B*, 1996, **54**, 11169–11186.

29 J. Perdew, K. Burke and M. Ernzerhof, *Phys. Rev. Lett.*, 1996, **77**, 3865–3868.

30 S. Dudarev and G. Botton, *Phys. Rev. B*, 1998, **57**, 1505–1509.

31 M. García-Mota, M. Bajdich, V. Viswanathan, A. Vojvodic, A. T. Bell and J. K. Nørskov, *J. Phys. Chem. C*, 2012, **116**, 21077–21082.

32 M. Bajdich, M. García-Mota, A. Vojvodic, J. K. Nørskov and A. T. Bell, *J. Am. Chem. Soc.*, 2013, **135**, 13521–13530.

33 E. Nurlaela, H. Wang, T. Shinagawa, S. Flanagan, S. Ould-Chikh, M. Qureshi, Z. Mics, P. Sautet, T. Le Bahers, E. Cánovas, M. Bonn and K. Takanabe, *ACS Catal.*, 2016, **6**, 4117–4126.

34 S. N. Steinmann and C. Corminboeuf, *J. Chem. Phys.*, 2011, **134**, 044117.

35 S. N. Steinmann and C. Corminboeuf, *J. Chem. Theory Comput.*, 2011, **7**, 3567–3577.

36 J. Chivot, L. Mendoza, C. Mansour, T. Pauporté and M. Cassir, *Corros. Sci.*, 2008, **50**, 62–69.

37 K. Mathew, R. Sundararaman, K. Letchworth-Weaver, T. A. Arias and R. G. Hennig, *J. Chem. Phys.*, 2014, **140**, 084106.

38 https://github.com/henniggroup/VASPsol.

39 K. Mathew, V. S. C. Kolluru, S. Mula, S. N. Steinmann and R. G. Hennig, *J. Chem. Phys.*, , DOI:10.1063/1.5132354.

40 C. D. Taylor, S. A. Wasileski, J. S. Filhol and M. Neurock, *Phys. Rev. B*, 2006, **73**, 1–16.

41 Y. M. Hajar, L. Treps, C. Michel, E. A. Baranova and S. N. Steinmann, *Catal. Sci. Technol.*, 2019, **9**, 5915–5926.

42 G. Henkelman and H. Jónsson, *J. Chem. Phys.*, 2000, **113**, 9978–9985.

43 G. Henkelman and H. Jónsson, *J. Chem. Phys.*, 1999, **111**, 7010–7022.

44 A. Heyden, A. T. Bell and F. J. Keil, *J. Chem. Phys.*, , DOI:10.1063/1.2104507.

45 J. Kästner and P. Sherwood, *J. Chem. Phys.*, 2008, **128**, 014106.

46 R. L. Doyle, I. J. Godwin, M. P. Brandon and M. E. G. Lyons, *Phys. Chem. Chem. Phys.*, 2013, **15**, 13737.

47 Y. H. Fang and Z. P. Liu, *ACS Catal.*, 2014, **4**, 4364–4376.

48 M. Van Den Bossche, E. Skúlason, C. Rose-Petruck and H. Jónsson, *J. Phys. Chem. C*, 2019, **123**, 4116–4124.

49 N. M. Marković, B. N. Grgur and P. N. Ross, *J. Phys. Chem. B*, 1997, **101**, 5405–5413.

50 K. Chan and J. K. Nørskov, *J. Phys. Chem. Lett.*, 2015, **6**, 2663–2668.

51 S. N. Steinmann and P. Sautet, *J. Phys. Chem. C*, 2016, **120**, 5619–5623.

52 P. Wang, S. N. Steinmann, G. Fu, C. Michel and P. Sautet, *ACS Catal.*, 2017, **7**, 1955–1959.

53 Y. Hajar, L. Treps, C. Michel, E. Baranova and S. Steinmann, *Catal. Sci. Technol.*, 2019, 10.1039/c9cy01421g.

54 A. Bergmann, T. E. Jones, E. Martinez Moreno, D. Teschner, P. Chernev, M. Gliech, T. Reier, H. Dau and P. Strasser, *Nat. Catal.*, 2018, **1**, 711–719.

55 M. Zhang, M. De Respinis and H. Frei, *Nat. Chem.*, 2014, **6**, 362–367.

56 S. N. Steinmann, C. Michel, R. Schwiedernoch, J. S. Filhol and P. Sautet, *ChemPhysChem*, 2015, **16**, 2307–2311.

57 C. Michel, J. Zaffran, A. M. Ruppert, J. Matras-Michalska, M. Jędrzejczyk, J. Grams and P. Sautet, *Chem. Commun.*, 2014, **50**, 12450–12453.

58 B. Schweitzer, S. N. Steinmann and C. Michel, *Phys. Chem. Chem. Phys.*, 2019, **21**, 5368–5377.

59 C. Lee, K. Shin, C. Jung, P.-P. Choi, G. Henkerlman and H.-M. Lee, *ACS Catal.*, 2019, DOI: 10.1021/acscatal.9b02249.